Vol. 18, No. 2 (2019) 555-569
Revista Mexicana de Ingeniería Química

EFFECTS OF RADIATION OF CO_2 LASER ON NATURAL DOLOMITE FOR THE DEGRADATION OF AZO DYE REACTIVE BLACK 5 BY PHOTOCATALYSIS

ESTUDIO DE LOS EFECTOS PROVOCADOS POR LA RADIACIÓN DEL LÁSER DE CO_2 EN LA DOLOMITA NATURAL, PARA LA DEGRADACIÓN DEL COLORANTE REACTIVO NEGRO 5 UTILIZANDO LA TÉCNICA DE FOTOCATÁLISIS

E. Márquez-Ramírez[1], A. Michtchenko[1], G. Zacahua-Tlacuatl[2]*

[1]*Instituto Politécnico Nacional, SEPI-ESIME-Zacatenco, Av. IPN S/N, Ed. 5, 3er. piso, Ciudad de México, C.P. 07738, México.*
[2]*Instituto Politécnico Nacional, Laboratorio de Posgrado e Investigación-ESIQIE, UPALM, Zacatenco, Av. IPN S/N, Ciudad de México, C.P. 07738, México.*

Received: October 17, 2018; Accepted: March 5, 2018

Abstract

In the present work, changes in Natural Dolomite (ND) produced by calcination using a CO_2 (carbon dioxide) laser radiation were analysed, as well as the effect on the degradation and decolourisation of the dye, Reactive Black 5 (RB5), when ND was used as a catalyst. The power density of the CO_2 laser and the duration of irradiation was varied. A mineral analysis was carried out using a scanning electron microscopy (SEM), energy-dispersive spectroscopy (EDS), and X-ray diffraction (XRD). The EDS analysis revealed the presence of elements such as magnesium (Mg), silicon (Si), aluminium (Al), calcium (Ca), oxygen (O), iron (Fe), zinc (Zn) and sodium (Na), while the X-ray diffraction analysis suggested that the treated dolomite samples experienced changes in their crystalline structure when calcined with the CO_2 laser. However, there were no changes in the main phase of the dolomite. Additionally, a photocatalytic study was performed on the degradation and decolourisation of the RB5 in an acid aqueous medium, using ND and ND calcined with the CO_2 laser radiation. Ultraviolet-visible spectrophotometry (UV/VIS) was used for the characterisation of the photocatalytic tests. An increase of 20% in the decolourisation and 19.6% in the degradation of the RB5 was observed.

Keywords: dolomite, black 5, photocatalysis, CO_2 laser, laser radiation.

Resumen

En el presente trabajo, se analizaron los cambios en la Dolomita Natural (DN) producidos por la calcinación con radiación de láser de CO_2 (dióxido de carbono), asimismo, el efecto en la degradación y decoloración del Colorante Reactivo Negro 5 (CN5) al utilizar DN calcinada como catalizador. Se variaron la densidad de potencia y el tiempo de radiación del láser de CO_2. Se analizó mediante microscopía electrónica de barrido (MEB), espectroscopia de dispersión de energía (EDS) y difracción de rayos X (DRX). El análisis EDS reveló la presencia de los elementos magnesio (Mg), silicio (Si), aluminio (Al), calcio (Ca), oxígeno (O), hierro (Fe), zinc (Zn) y sodio (Na), mientras que el análisis de DRX sugirió cambios en la estructura cristalina de la DN cuando fue calcinada, sin embargo, la fase principal de la DN se conservó. Además, se realizó un estudio fotocatalítico para la degradación y decoloración del CN5 en un medio acuoso ácido usando DN y DN calcinada con radiación de láser de CO_2. Se utilizó la espectrofotometría ultravioleta-visible (UV/VIS) para la caracterización de las pruebas. Se observó un aumento del 20% en la decoloración y un 19.6% en la degradación del CN5.

Palabras clave: dolomita, negro 5, fotocatálisis, CO_2 láser, radiación láser.

1 Introduction

Currently, there are more than 10,000 types of synthetic dyes commercially available, which are used in the textile, cosmetic, food, medicine, and other industries. The annual production worldwide is approximately 700,000 tons of dyes are produced yearly (Zollinger *et al*., 1987). Of this amount, approximately 10-15% of the dyes are released into the environment during manufacturing and usage (Vaidya *et al*., 1982; Sheet *et al*., 2014).

* *Corresponding author. E-mail*: gzt388@gmail.com
Tel. 57296000 Ext. 55124
https://doi.org/10.24275/uam/izt/dcbi/revmexingquim/2019v18n2/Marquez
issn-e: 2395-8472

Nowadays, the estimated production of colourants worldwide is about 10 million tons yearly, with azo dyes being the most used ones in the textile industry, representing approximately 70% of this production (Behnajady *et al*., 2007; Mahmoodi *et al*., 2006). These types of dyes are chemically stable because they contain an azo group, consisting of two nitrogen atoms (−N=N−), so they are considered poorly biodegradable. Thus, most of the residual dyes accumulate in lakes and bays and cause a decrease in the amount of sunlight passing through the water, and consequently, induces a decrease in the photosynthetic activity. This in turn decreases the available oxygen content in the ecosystems (Lucas *et al*., 2006; Kaneva *et al*., 2016). Traditional wastewater treatments have proved to be remarkably ineffective in the handling of wastewater of the synthetic textile dyeing process, because the treatment of industrial waters can be complicated by the containing of recalcitrant or refractory compounds, whose biological degradation occurs so slowly that it makes inefficient this type of system (Salas. 2010). Other investigations have also addressed this problem using different processes, such as activated carbon absorption (Nematollahzadeh *et al*., 2015; Al-Degs *et al*., 2007; Ip. Barford *et al*., 2010; Vinod *et al*., 2014; Tawfik *et al*., 2014), filtration (Ahmad *et al*., 2007); by means of mesoporous carbon (Mohammadi *et al*., 2011), using immobilised white rot fungi cells (Martinez. 2017), by core/cell nanoparticles (Vinod *et al*., 2014), synthesising copper nanoparticles (Manoj *et al*., 2016), with nanocomposites (Saravanan *et al*., 2013-2015), using polyamide nanocomposite membrane, containing alumina nanoparticles synthesised in situ with interfacial polymerisation (Tawfik *et al*., 2012), the removal of hazardous dyes and others compounds using graphene oxide (Robati *et al*., 2016), by ultrasonic-assisted adsorption (Ghaedi *et al*., 2015; Arash *et al*., 2015), oxidisation and degradation (Domenzain *et al*., 2016), and finally utilising rice husk and its ash as low-cost adsorbents in water and wastewater treatment (Ahmaruzzaman *et al*., 2011), are some common examples. Even though there are another processes as well, such as an adsorptive removal of dyes through carbon nanotubes; however, it has been observed that these kinds of processes have toxic effects (Vinod *et al*., 2013). There is also the biosorption process for wastewater treatment but it is focused on the concentration of metal (Vinod et al 2015). Additionally, some researchers have addressed most of the dyes, in particular, the azo dyes, contain carcinogenic properties (Golka *et al*., 2004).

Studies on advanced oxidation process (AOPs) have demonstrated that it can be a potential technological alternative for the treatment of effluents. AOPs is based on the generation of hydroxyl radicals (OH•), which are highly oxidant and non-selective, promoting the degradation of extremely polluting compounds and contributing to their total mineralisation. The OH• radicals can modify the chemical structure of recalcitrant organic compounds, converting them into simpler compounds with lower molecular mass, contributing to less toxicity for micro-organisms and consequently higher biodegradability (Muruganandham *et al*., 2004; Giraldo *et al*., 2004). Within the AOPs, photocatalysis is another technique often used to accelerate the generation of OH• radicals through photoreaction. It combines hydrogen peroxide compounds (H_2O_2) with white light, thereby containing the ability to accelerate the production of OH• radicals (Vinod *et al*., 2011; Saravanan *et al*., 2013). The mechanism occurs through the action of emitted radiation by a white light lamp for the photolysis of H_2O_2 molecules, meaning that the molecule is broken down by photons producing OH• radicals, as is expressed in Eq. (1).

$$H_2O_2 + h\nu \rightarrow 2OH\bullet \quad (1)$$

Heterogeneous photocatalysis is a catalytic phenomenon, related to the chemical properties existing at the surface of a solid. It is associated with the adsorption of molecules of a fluid on the surface of a solid, so the oxidation directly takes place on the surface of the particle that is used as a catalyser. Every solid has the property to fix or adsorb the nearby molecules, atoms, or ions on its surface. Adsorption can be produced either by breaking a crystal or using the van der Waals forces. On one hand, the process of breaking a crystal consists the breaking of some covalent bonds, providing one or more free valences to each atom of the surface. The number of nearby atoms existing on the crystal, before the surface formation, generates a decrease, experiencing a set of unbalanced forces; this phenomenon is known as surface free energy. If a molecule with an affinity with these free valences is close enough, an electronic arrangement will occur with the system, similar to that exhibited in a chemical reaction. The result is the fixation of the molecule to the surface, through chemical adsorption or chemisorption. On the other hand, the other recognised form of adsorption is one occurring through the van der Waals forces between atoms, molecules, and the surface. In this case, there is not an electronic arrangement in the system but there are

forces produced by electronic or dipolar attractions. This type of interaction is called physical adsorption or physisorption (Fuentes *et al*., 1997; Gelover *et al*., 2014).

The catalytic activities are strongly dependent on the composition, size, and shape of the catalyst. In the photocatalytic technique, irradiation of the semiconductor with a photon of sufficient energy, greater or equal to the band gap energy, could promote an electron from a valence band to a conduction band. As a result, the electron leaves a vacancy behind in the valence band called positive holes, which could oxidise the organic material by the removal of an electron or react with water or hydroxyl forming a powerful oxidant; a hydroxyl radical, as can be seen in Fig. 1. The conduction band electrons reduce dissolved oxygen, producing a superoxide anion radical, which is highly reactive and can oxidise any organic compound (Tawfik *et al*., 2011; Saravanan *et al*., 2016).

The Fenton system is one of the most utilised systems, degrading various azo dyes with the hydroxyl radical, generated from the reduction of hydrogen peroxide molecules with Fe (II) ions at acid pH:

$$Fe^{2+} + H_2O_2 \rightarrow Fe^{3+} + OH^- + OH\bullet \quad (2)$$

$$Fe^{3+} + H_2O_2 \rightarrow Fe(OOH)^{2+} + H^+ \quad (3)$$

$$Fe(OOH)^{2+} \rightarrow Fe^{2+} + HO_2\bullet \quad (4)$$

The presence of light radiation in the photo Fenton process improves the azo dye degradation efficiency, due to quick photoreduction of the ferric ion to ferrous ion (Vergara *et al*., 2012; Karthikeyan *et al*., 2012). The oxidative decolourisation of RB5 has been previously studied, using the processes of Fenton and photo-Fenton, which were found to be effective. Also, the use of mercury lamps at low pressure have been investigated for this purpose.

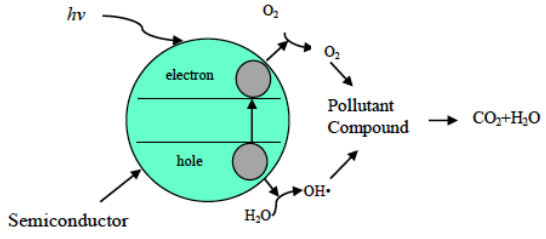

Fig. 1. Scheme of formation of the redox pair in a particle of the semiconductor..

They exhibited minimal effect in decolourisation, but they were effective for the mineralisation of dyes; the H_2O_2 was also studied. Without the combination with other reagents, it had no influence on the decolourisation of the dye. However, in concentrations of 2.4×10^{-4} to 9.8×10^{-4} mol/L, it increased the decolourisation. Moreover, some researchers have found that the pH of the dye solution has an important impact on the adsorption capacity, significantly the extent of adsorption of the dye is affected, due to the effect of pH on the surface binding sites of the adsorbent, and on the ionisation processes of the dye molecules. An optimum pH of 3 was selected for further investigation. The higher adsorption of the dye, at a low pH is apparently due to greater accessibility of the dye to active sites and more facile diffusion (Mittal *et al*., 2010; Hadi *et al*., 2010). Additionally, some investigations for the treatment of contaminated affluent have been carried out using porous materials, either as absorbents or as a catalyst support. For instance, the natural zeolite, which is a porous material calcined at different temperatures, has demonstrated a decolourisation between 80% and 85% and elimination of 50% of RB5 dye. These properties are ascribed to it due to its composition of semiconductors, namely, iron, titanium and zinc (Domenzain *et al*., 2016). Semiconductors are the commonly used materials in the degradation process of azo dyes. There are several approaches to improve the photocatalytic activity of semiconductors under visible light, such as dye sensibilisation, polymer sensitisation, non-metal doping, metal doping, and coupling of semiconductors. Doping is a generally used method to improve the various properties of semiconductors (Saravanan *et al*., 2013). Furthermore, Dolomite has been investigated for these purposes. It is a double carbonate of calcium and magnesium, $CaMg(CO_3)_2$, containing 30.41% of CaO, 21.86% of MgO, and 47.73% of CO_2 in its purest forms. It is formed by rhombohedral crystals, which are usually deformed. It is very crushed, curved, and compacted in the form of small geodes (dolomites). Usually, it may contain impurities, such as Fe and Mg. Due to its Fe content and porosity, it can be a good catalyst. Fe as an active phase is responsible for the catalytic activity, while the porosity disperses the active phase, stabilising and providing good mechanical properties (Muruganandham *et al*., 2004; Giraldo *et al*., 2004; Fuentes *et al*., 1997).

Some investigations have shown that calcined

dolomite has improvements in its composition and high capacities of absorption when the dolomite is decarbonised through calcination, it produces MgO and increases its specific area, which has been shown to be the main contributor to the elimination of boron (B) (Sasaki *et al*., 2013). Some of the applications of calcined dolomite are for the treatment of phosphate waters, pentachlorophenol, chromate (Albadarin *et al*., 2012), Pb^{2+}, and reactive dyes (Dobrowolski *et al*., 1999).

In particular, the CO_2 laser radiation is one of the most used because it is highly efficient, with a high concentration of energy and a potential source of heat due to its monochromatic beam. Also, it has been used to process materials for grain refinement, homogenisation, increasing corrosion and fatigue resistance, and enhancing the micro-hardness in aluminium and titanium alloys (Nagarathnam. 2001; Dutta *et al*., 2003) as well as being used for improving the mechanical properties in fresh cement paste, by producing fewer pores (Moreno *et al*., 2011).

The objective of this work was to determine the effects of CO_2 laser radiation on the properties of the ND, and its subsequent use as a catalyst in the degradation and decolourisation of RB5. This material was characterised to determine its global composition, the inner phases, and the presence of iron oxides in the mineral, which is a promoter for the elimination of the RB5 dye using the photocatalysis process. It is also used to identify the power and the duration of irradiation that provides the dolomite better features as a catalyst.

The novelty of this work was to change the conventional way of calcining which is usually done with muffles, the conventional calcination can take hours and generate a considerable expenditure of energy, so it has been proposed to replace the calcination with muffle by calcination with CO_2 laser radiation, which contributes to a considerable saving of energy and time, in addition to the use of dolomite as a catalyst for the degradation of azo dyes.

2 Materials and methods

Natural dolomite (ND) in powder was used for the samples. The dolomite used was from Catano-Etla, Oaxaca, México. The zone is corresponding to the Miocene age, approximately from 15 million years (Dobrowolski *et al*., 1999). The azo dye, Reactive Black 5 (RB5) supplied by Ciba-Geigy® was used for the photocatalytic process. Hydrogen peroxide (H_2O_2) stabilized at 30% was used as an oxidizing agent while chlorhydric acid was employed to control the pH of the solution; both compounds were supplied by Fermont®. A commercial light lamp of 25 Watts provided by Tecno Lite® was used to radiate the aqueous solution.

The ND was calcined by using a CO_2 laser radiation of 130 Watts with a wavelength of 10.6 μm. The power densities used were $I = 1.18 \times 10^6$ W/m^2, $I = 1.33 \times 10^6$ W/m^2 and $I = 1.49 \times 10^6$ W/m^2 applied at time periods of 5, 10 and 15 s. Thus, nine calcined samples and one more without calcining, denominated as the control sample (CS) were prepared, see Table 1.

The laser set-up used for the calcination process is illustrated in Fig. 2. The important property of the laser treatment is the power density, which determines the kind of laser treatment, represented in the Eq. (5). (Pawlowski. 1999):

$$I = \frac{P}{S} \tag{5}$$

where I is the laser power density, P is the laser output power and S is the beam area.

Table 1. Parameters used for the preparation of the samples.

Sample	Power density $\times 10^6$ [W/m^2]	Calcination time [s]
CS	-	-
S1	1.18	5
S2	1.18	10
S3	1.18	15
S4	1.33	5
S5	1.33	10
S6	1.33	15
S7	1.49	5
S8	1.49	10
S9	1.49	15

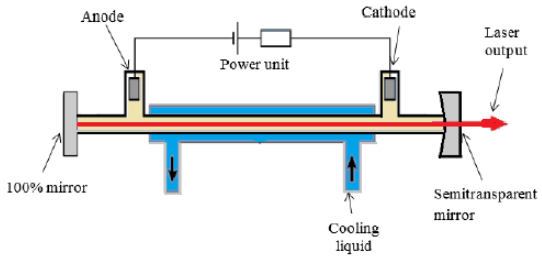

Fig. 2. CO_2 laser set-up used to radiate samples of natural dolomite.

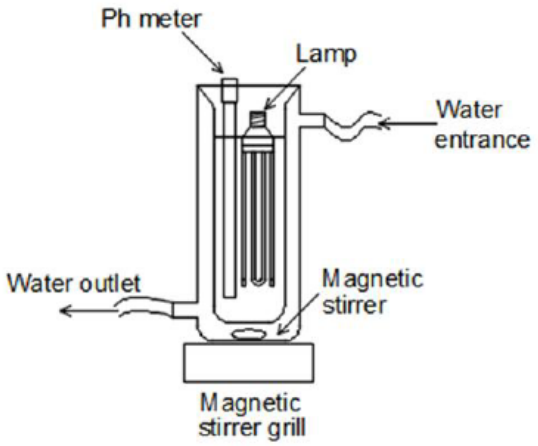

Fig. 3. Schematic view of the photocatalytic reactor assembly.

Furthermore, the ND was evaluated as a catalyser using RB5. For this, H_2O_2 was used as an oxidising agent and hydrochloric acid to control the pH at 2.5. The aqueous solution was made of 250 ml of distilled water with 50 ppm of RB5 and 20 ppm of each sample, respectively. The solution was constantly agitated using a rotary magnetic bar, keeping a temperature of 20 ºC for the whole experiment. The reactor assembly used can be seen in Fig. 3. The reactor was coated with aluminium foil to constrain the light inside the reactor. The spectral data of the catalytic activity were obtained using a UV/VIS variant spectrophotometer, model Cary 1 G, at a scanning speed of 600 nm/min and a wavelength range of 190 to 900 nm. The degradation of RB5 was monitored for 100 minutes, with 10 minutes intervals for each aliquot. This process was conducted for the ten samples considered.

3 Results and discussion

3.1 Energy-Dispersive X-Ray Spectroscopy (EDS)

According to the results obtained by the EDS, the sample was found to be mainly composed of O, Mg, Ca, Si, and Al. Moreover, Si and Al were at the highest percentages meanwhile Na, Fe, copper (Cu) and potassium (K) were at the lowest. The natural sample used had great potential as a catalyser due to its Fe content and porosity.

The results of the EDS analyses for each sample can be seen in Tables 2-4 and Figs. 4-6. The results suggest that the effect of calcination at different power densities and different times did not alter the chemical elements present. However, the percentage weight of each element showed a slight increase. The increase can be attributed to the fact that there was oxidation by the laser heating, producing the combustion of a substance.

The content of Ca and Mg increases for the calcined samples. The Ca/Mg ratio, called relative sensitivity factor, was higher than 1, which suggests that the crude sample was not only composed of dolomite but it also contained other minerals o phases (Sasaki *et al*., 2013).

Table 2. Percentage weight of the chemical elements obtained by EDS, for a power density of $I = 1.18 \times 10^6$ W/m^2.

Elements	CS	S1	S2	S3
	Weight [%]			
		5 s	10 s	15 s
O K	50.08	47.01	47.58	49.1
Na K	2.97	0.66	0.75	1.11
Mg K	7.23	6.84	6.31	7.01
Al K	6.03	5.37	5.7	5.32
Si K	14.91	16.5	16.88	16.11
K K	1.3	2.15	2.37	2.11
Ca K	8.01	13.74	13.27	13.76
Fe K	1.42	3.03	3.06	2.7
Cu K	4.4	2.66	2.35	2.77
Zn K	3.64	2.04	1.73	1.96
Ca/Mg	1.11	2.01	2.1	1.96

Table 3. Percentage weight of the chemical elements obtained by EDS, for a power density of $I = 1.33 \times 10^6$ W/m^2.

Elements	CS	S4	S5	S6
	Weight [%]			
		5 s	10 s	15 s
O K	50.08	48.87	47.38	52.93
Na K	2.97	1.14	0.78	0.56
Mg K	7.23	6.84	6.99	6.89
Al K	6.03	5.41	5.41	5.49
Si K	14.91	15.73	16.49	16.94
K K	1.3	2.1	1.98	2.45
Ca K	8.01	12.85	13.41	15.3
Fe K	1.42	2.45	2.66	2.97
Cu K	4.4	2.71	2.63	2.57
Zn K	3.64	1.9	2.26	2.36
Ca/Mg	1.11	1.88	1.92	2.22

Table 4. Percentage weight of the chemical elements obtained by EDS, for a power density of $I = 1.49 \times 10^6$ W/m^2.

Elements	CS	S7	S8	S9
	Weight [%]			
		5 s	10 s	15 s
O K	50.08	49.46	48.5	49.66
Na K	2.97	2.56	2.37	2.09
Mg K	7.23	7.3	7.63	7.66
Al K	6.03	5.78	5.94	5.8
Si K	14.91	16.21	16.44	15.91
K K	1.3	1.78	1.93	1.7
Ca K	8.01	11.85	12.06	12.03
Fe K	1.42	2.02	2.32	2.19
Cu K	4.4	2.95	2.97	2.61
Zn K	3.64	2.65	2.21	2.45
Ca/Mg	1.11	1.64	1.58	1.57

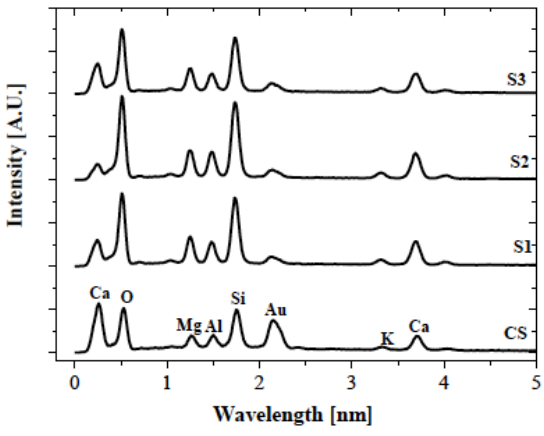

Fig. 4. Distribution of chemical elements obtained by EDS, for a power density of $I = 1.18 \times 10^6$ W/m^2.

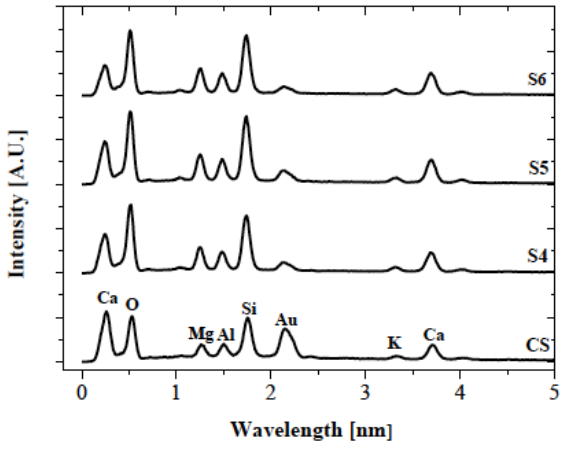

Fig. 5. Distribution of chemical elements obtained by EDS, for a power density of $I = 1.33 \times 10^6$ W/m^2.

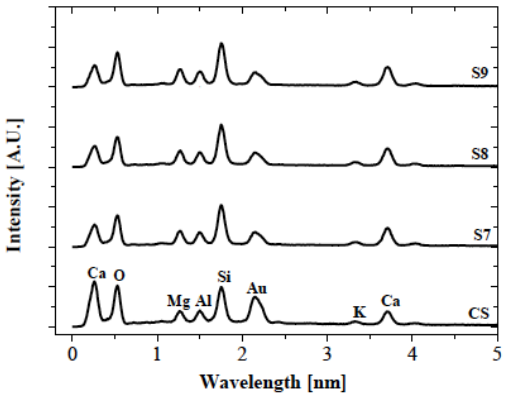

Fig. 6. Distribution of elements obtained by EDS, for a power density of $I = 1.33 \times 10^6$ W/m^2.

3.2 *Scanning Electron Microscopy (SEM)*

The structural microanalysis of the natural dolomite samples was carried out by SEM. The micrographs of S7, S8, S9, and CS samples are depicted in Fig. 7. It was found that the samples had considerable changes in their structure when they were calcined with the CO_2 laser radiation.

The best definition of morphology was obtained in the samples prepared at a power density of $I = 1.49 \times 10^6$ W/m^2 for 5, 10 and 15 s, while for the other samples it could not be distinguished. An increase in the porosity and structures, in the form of needles, flat platelets and cubes, and a high formation of particle agglomerates were identified. Also, a more compact structure of platelets and flakes was observed in S8. However, the increase of the structures in the form of needles was remarkable.

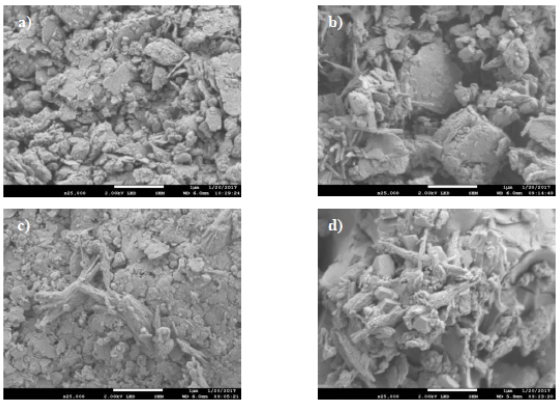

Fig. 7. Micrographs from the samples at $I = 1.49 \times 10^6$ W/m^2; a) SC; b) S7; c) S8; and d) S9.

This was possible due to the increase of the temperature, and the effect of the laser radiation, which suggests that each sample exhibited different structures and different sizes due to each particular calcination process.

3.3 *X-Ray diffraction*

The patterns of calcined and uncalcined ND, at power densities of $I = 1.18 \times 10^6$ W/m^2, $I = 1.33 \times 10^6$ W/m^2, and $I = 1.49 \times 10^6$ W/m^2, at 5, 10 and 15 seconds, are shown in Fig. 8.

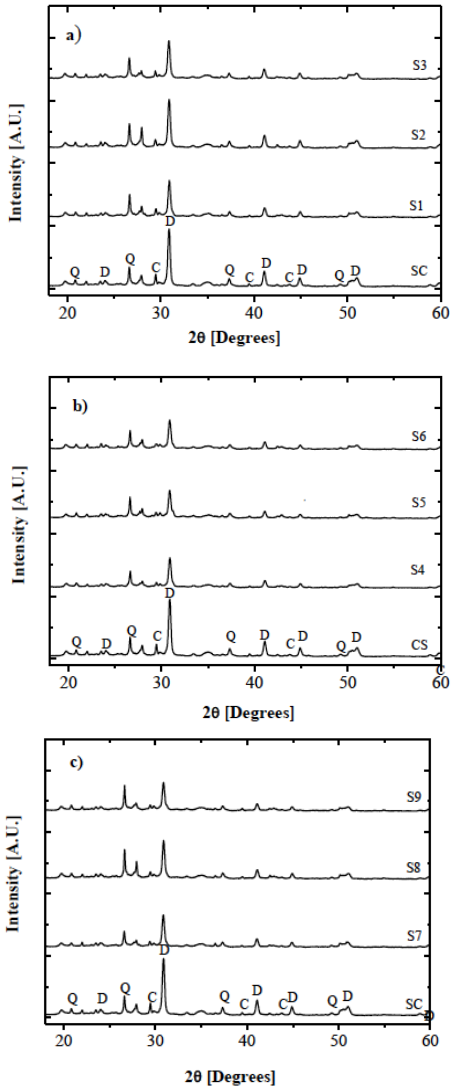

Fig. 8. Diffractograms for the samples prepared at different power intensities; a) $I = 1.18 \times 10^6$ W/m^2; b) $I = 1.33 \times 10^6$ W/m^2; c) $I = 1.49 \times 10^6$ W/m^2.

In the analysis, the main phase of dolomite was identified by the characteristic peaks, located in 2θ=30.90º and in 2θ=40.07º, the quartz phase, considered as impurities, was located in 2θ=26.62º and 2θ=50.10º; and the phase of calcite, also considered as an impurity, was identified in 2θ=29.40º and 2θ=48.51º. In the patterns, low crystallinity with a certain degree of amorphousness was observed. It was determined by the lack of linearity of the baseline of the diffractograms. Besides, it was found that the intensities of the signals changed, due to the increase in the calcination temperature when the samples were radiated, but there were no phase changes in the most intense signals located at 2θ=30.90º and at 2θ=40.07º. These signals also decreased, which can be seen in Fig. 8a); b) and c). On the other hand, for the samples prepared at a power density of $I = 1.33 \times 10^6$ W/m^2. Furthermore, the only phase that showed a decrease in signal (intensity), corresponded to the dolomite. The calcite showed a slight decrease in intensity, while the intensity of quartz was not affected signalling to the characteristic phase.

3.4 Calculation of crystal size

The Debye-Scherrer method was used for the crystal size determination, which is generally used to determine the mean diameter of a crystal grain, in the most representative phases involved in the sample studied. For this, one peak was analysed for the dolomite phase and another for the quartz phase. The peak analysed for the dolomite phase, corresponded to the diffraction angle existing in 2θ=30.90°, meanwhile for the quartz phase it was in 2θ=26.62°, as seen in Fig. 9.

Table 5. The crystal size of the dolomite and quartz phases.

Sample	Dolomite crystal size	Quartz crystal size
	(nm)	(nm)
SC	26.76	55.26
S1	26.25	59.27
S2	26.42	58.25
S3	26.32	56.48
S4	25.35	51.79
S5	25.58	57.69
S6	25.59	57.13
S7	25.92	51.53
S8	26.71	64.51
S9	26.45	61.68

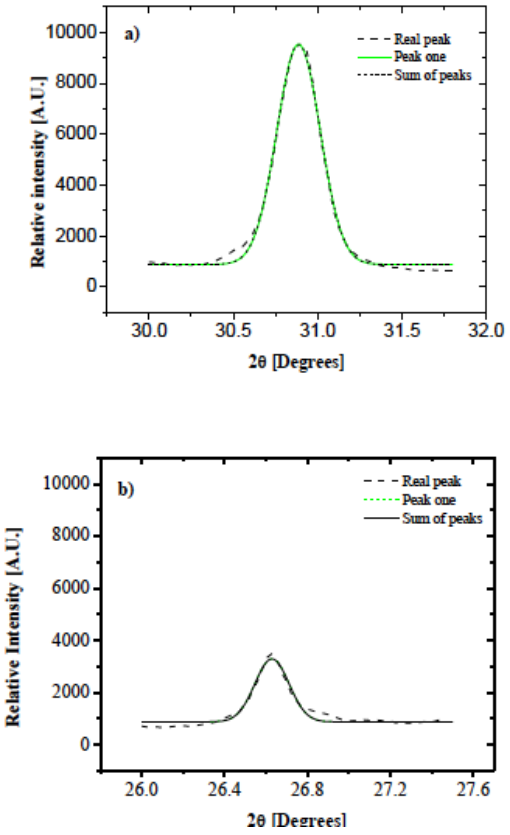

Fig. 9. Diffraction pattern simulation adjusted with a Gaussian distribution; a) 2θ=30.9° for the dolomite phase; b) 2θ=26.62° for the quartz phase.

It shows an example of the data obtained for the CS by this method. The results obtained for each sample are reported in Table 5. In both cases, they were adjusted with a Gaussian distribution. To determine the crystal size, Eq. 6 was used.

$$D = \frac{K\lambda}{\beta \times \cos\theta} \tag{6}$$

where D is the crystal diameter, λ is the X-ray wavelength equal to 0.154 nm, K is the shape factor with a value of 0.89, β is the full width at half maximum FWHM in radians units and θ is the angle measured in degrees.

According to the results obtained for the dolomite crystal diameter, a general behaviour was observed. A slight decrease of particle size for the samples, prepared at $I = 1.33 \times 10^6$ W/m^2 (S4, S5, and S6 samples), with the smallest diameter was found, which means that the crystal size can be reduced by increasing the temperature. On the other hand, for the quartz phase, it showed a slight increase in most cases.

3.5 UV/VIS spectroscopy

The UV/VIS spectroscopy technique was used to measure the changes in the absorption bands of RB5 to determine degradation and decolourisation. The process was monitored and evaluated by changing the spectral signals as a function of the reaction time. The hydroxyl radical generated during the photocatalytic process continuously attacked the organic pollutant, through a series of reactions. In this process, the complex organic structure of the pollutant is broken down into smaller intermediates compounds. Moreover, the azo-bond (C−N=N−) is attacked during the photocatalytic dye degradation process, and this destruction of the C−N and N=N bonds leads to colour removal. (Gelover *et al.*, 2014; Stambolova *et al.*, 2012; Aguedach *et al.*, 2005; Damodar *et al.*, 2010; Bauer *et al.*, 2001).

3.5.1 Decolourisation of RB5 dye at the 595 nm band

In Fig. 10, the calibration curve of RB5 is shown. It was generated from different solutions, within the range of 10 ppm to 100 ppm, with intervals of 10 ppm. The amount of light absorbed was measured using a UV/VIS spectrophotometer. The absorption peak at 595 nm, in the visible region, was the band analysed for the chromophores, containing a conjugated π bond using two double azo bonds of the RB5 group, which were used to measure the decolourisation.

The concentration of the colourant in the solution was calculated with the Lambert-Beer law. The values were obtained by segmenting the UV-VIS spectra in a calibration graph at λ = 595 nm.

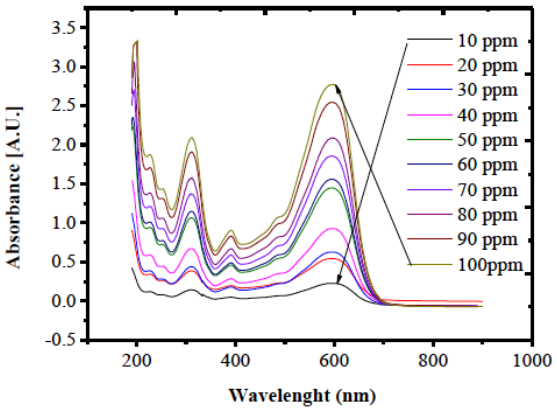

Fig. 10. UV-Visible absorption spectra of RB5 solution during degradation by photocatalysis.

The percentage of decolourisation (*%Decolourisation*) was calculated by means of Eq. 7 (Dutta *et al.*, 2003; Moreno, 2011; Lucas *et al.*, 2006; Saravanan *et al.*, 2013):

$$\%Decolourisation = \left(1 - \frac{C}{C_0}\right) \times 100 \qquad (7)$$

where C is dye concentration (ppm) at the beginning and C_0 is dye concentration at a determined time. Table 6 summarises all the results in percentage for decolourisation at 595 nm and degradation at 310 nm for each of the calcined samples and the control sample.

Fig. 11a shows the results obtained for the samples prepared at $I = 1.18 \times 10^6$ W/m^2. It was observed that the highest percentage of removal was caused in the S2 sample.

Table 6. Percentage of degradation and decolourisation, according to a density of power and duration of irradiation (calcination).

Sample	Power density	Irradiation time	Decolourisation (λ = 595 nm)	Degradation (λ = 310 nm)
	[W/mm^2]	[s]	[%]	[%]
MC	-	-	67.8	37.8
S1	1.18	5	72.4	36.6
S2	1.18	10	80.7	45.8
S3	1.18	15	72.4	46.7
S4	1.33	5	76.9	46.7
S5	1.33	10	75.6	42.5
S6	1.33	15	86	53.4
S7	1.49	5	72.6	45.2
S8	1.49	10	44	73.9
S9	1.49	15	87.9	57.4

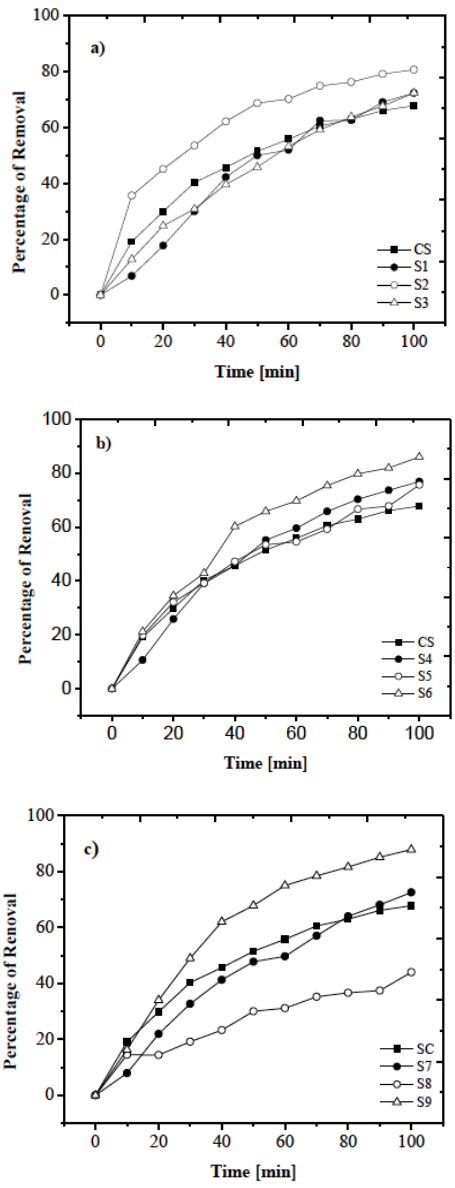

Fig. 11. Comparison of the percentage of removal of samples radiated at different times: 5, 10 and 15 seconds against the control sample for λ = 595 nm at different power densities: a) $I = 1.18 \times 10^6$ W/m^2; b) b) $I = 1.33 \times 10^6$ W/m^2 and c) $I = 1.49 \times 10^6$ W/m^2.

The percentage of decolourisation of this sample was approximately 80.70%. On the other hand, the S1 and S3 samples demonstrated a decolourisation percentage of approximately 72.40% for the RB5, similar to the decolourisation exhibited for CS. In the case of the samples radiated at $I = 1.33 \times 10^6$ W/m^2, see Fig. 11b, only the sample S6 presented the highest percentage of removal at 86%; however, the decolourisation kept improving until 50 min of the reaction was completed. The S4 and S5 samples showed 76.9% and 75.6% of decolourisation respectively. Finally, the results for the samples radiated at $I = 1.49 \times 10^6$ W/m^2 are shown in Fig. 11c. It was observed that the S9 sample exhibited a percentage removal of 87.9%, which was to the highest in comparison with the S7 and S8 samples, presenting percentages of 72.6% and 44%, respectively. The S8 sample was less efficient than CS due to the fact that the sample collapsed in presenting inefficient behaviour as a catalyser.

3.5.2 *Degradation of RB5 dye at the 310 nm band*

The peaks at 310 nm in the UV region were related to the naphthalene rings. In this case, the degradation of the two aromatic structures were also identified, which are assigned to the $\pi-\pi$ transition of an electron, (Damodar *et al*., 2010).

The degradation values for each of the samples were obtained by segmenting the UV-VIS spectra in the calibration graph for the degradation peaks at 310 nm. The percentage of degradation (*%Degradation*) was calculated using Eq. 8, (Tawkik *et al*., 2012; Luna *et al*., 2013; Savaranan *et al*., 2013).

$$\%Degradation = \left(1 - \frac{C}{C_0}\right) \times 100 \qquad (8)$$

where C is dye concentration (ppm) at the beginning, and C_0 is dye concentration at a determined time.

Fig. 12 shows the degradation behaviour of RB5, using the samples studied. In Fig. 12a the behaviour for the samples prepared at the density of $I = 1.18 \times 10^6$ W/m^2 are shown, the performance was similar for the two samples: S2 and S3, with 45.80% and 46.70% respectively. The least efficient sample was S1, presenting a degradation percentage of 36.60%. It was due to the low radiation time and the low laser power used. In Fig. 12b, the samples were prepared at the density of $I = 1.33 \times 10^6$ W/m^2. It can be seen that better behaviour was achieved by S6, with 53.4% of degradation. In Fig. 12c, the degradation achieved in the sample S8, with a power density of $I = 1.49 \times 10^6$ W/m^2, can be seen to be 73.90%.

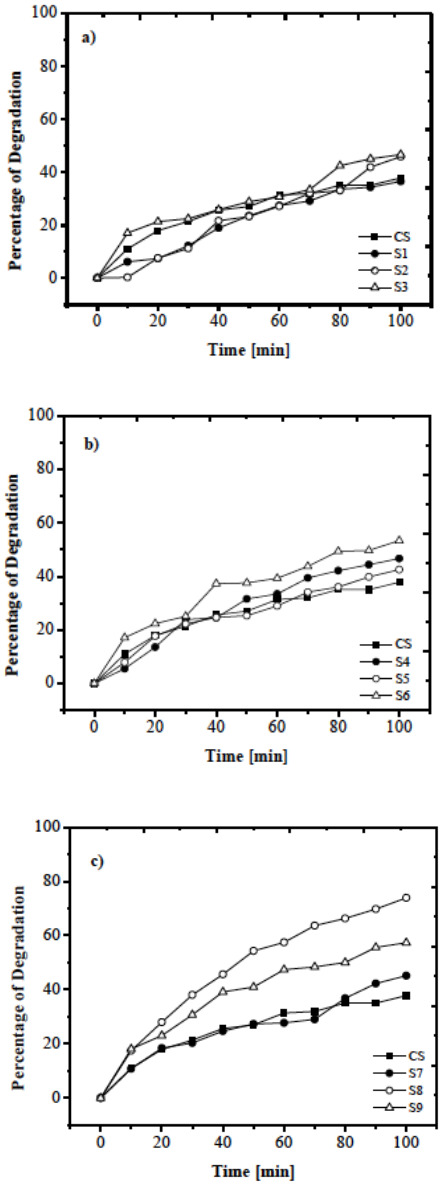

Fig. 12. Comparison of degradation behavior of the samples radiated at the same power density at: a) $I = 1.18 \times 10^6$ W/m^2, b) $I = 1.33 \times 10^6$ W/m^2 and c) $I = 1.49 \times 10^6$ W/m^2.

Conclusions

The use of photocatalysis processes with calcined dolomite, hydrogen peroxide, and white light for decolourisation and degradation of RB5, may represent an opportunity for new applications of the CO_2 laser radiation, and also for dolomite, since, this material is abundant in nature; it is suitable for its characteristics and its low cost. It was found that the CO_2 laser radiation of is effective for the calcination of ND, since, the results showed that there was greater decolourisation and degradation of the RB5 when ND calcined with CO_2 laser radiation was used as a catalyst than when ND was used without calcining. The increment was of 20% more in the decolourisation and 19.60% more in the degradation of the RB5 in comparison to the results obtained when the ND without calcining was used. It was seen in the results that the best decolourisation was obtained with the sample that was calcined at a higher power density and with longer irradiation time. On the other hand, the crystal size for the dolomite was maintained in a range of 25.32 nm to 26.76 nm while the range for the crystal size for the quartz was 51.53 nm to 64.51 nm. A more in-depth analysis must be performed that includes aspects of the longest irradiation time and largest irradiation areas, as well as an economic feasibility analysis that determines the potential of this alternative option.

Acknowledgements

The authors gratefully acknowledge Consejo Nacional de Ciencia y Tecnología (CONACYT) for supported this work, Instituto Politécnico Nacional (México), Centro de Nanociencias y Micro y Nanotecnologías-IPN (CNMN-IPN) and Escuela Superior de Ingeniería Química e Industrias Extractivas-IPN (ESIQIE-IPN).

Abbreviations

I	laser power density, W/m^2
P	laser output power, W
S	beam area, m^2
D	crystal diameter, nm
K	shape factor
C	is dye time concentration at the beginning, ppm
C_0	is dye concentration at a determined, ppm
H_2O_2	hydrogen peroxide
OH•	hydroxyl radicals
Fe	Iron
AOPs	Advanced Oxidation Process
RB5	Reactive Black 5
ND	Natural Dolomite
s	seconds
ppm	Parts per million

Greek symbols

λ	wavelenght
β	full width at half maximum: FWHM
θ	angle, degrees
$h\nu$	energy of a photon

References

Aguedach, A., Brosillon, S., Morvan, J., and Lhadi, E. K. (2005). Photocatalytic degradation of azo-dyes reactive black 5 and reactive yellow 145 in water over a newly deposited titanium dioxide. *Applied Catalysis B: Environmental, 57*, 55-62. https://doi.org/10.1016/j.apcatb.2004.10.009

Ahmad, A. L., and Puasa, S. W. (2007). Reactive dyes decolourization from an aqueous solution by combined coagulation/micellar-enhanced ultrafiltration process. *Chemical Engineering Journal 132*, 257-265. https://doi.org/10.1016/j.cej.2007.01.005

Ahmaruzzaman, M., and Gupta, V. K. (2011). Rice husk and its ash as low-cost adsorbents in water and wastewater treatment. *Industrial and Engineering Chemistry Research 50*, 13589-13613. https://doi.org/10.1021/ie201477c

Al-Degs, Y., Khraisheh, M. A. M., Allen, S. J., Ahmad, M. N., and Walker, G. M. (2007). Competitive adsorption of reactive dyes from solution: Equilibrium isotherm studies in single and multisolute systems. *Chemical Engineering Journal 128*, 163-167. https://doi.org/10.1016/j.cej.2006.10.009

Albadarin, A. B., Mangwandi, C., Al-Muhtaseb, A. H., Walker, G. M., Allen, S. J., and Ahmad, M. N. M. (2012). Kinetic and thermodynamics of chromium ions adsorption onto low-cost dolomite adsorbent. *Chemical Engineering Journal 179* 193-202. https://doi.org/10.1016/j.cej.2011.10.080

Arash Asfaram , Mehrorang Ghaedi, Shilpi Agarwalb, Inderjeet Tyagib, V. K. G. (2015.). Removal af basic dye Auramine-O by ZnS: Cu nanoparticles loaded on activated carbon. Optimization of parameters using response surface methodology wish central composite design. *RSC Advances 5*, 18438-18450. https://doi.org/10.1039/C4RA15637D

Alvin, W. M., Barford, J. P., and McKay, G. (2010). A comparative study on the kinetics and mechanisms of removal of Reactive Black 5 by adsorption onto activated carbons and bone char. *Chemical Engineering Journal 157*, 434-442. https://doi.org/10.1016/j.cej.2009.12.003

Bauer, C., Jacques, P., and Kalt, A. (2001). Photooxidation of an azo dye induced by visible light incident on the surface of TiO_2. *Journal of Photochemistry and Photobiology A: Chemistry 140*, 87-92. https://doi.org/10.1016/S1010-6030(01)00391-4

Behnajady, M. A., Modirshahla, N., Daneshvar, N., and Rabbani, M. (2007). Photocatalytic degradation of an azo dye in a tubular continuous-flow photoreactor with immobilized TiO_2 on glass plates. *Chemical Engineering Journal 127*, 167-176. https://doi.org/10.1016/j.cej.2006.09.013

Devaraj, M., Saravanan, R., Deivasigamani, R., Gupta, V. K., Gracia, F., and Jayadevan, S. (2016). Fabrication of novel shape Cu and Cu/Cu_2O nanoparticles modified electrode for the determination of dopamine and paracetamol. *Journal of Molecular Liquids 221*, 930-941. https://doi.org/10.1016/j.molliq.2016.06.028

Damodar, R. A., and You, S. J. (2010). Performance of an integrated membrane photocatalytic reactor for the removal of Reactive Black 5. *Separation and Purification Technology 71*, 44-49. https://doi.org/10.1016/j.seppur.2009.10.025

Dobrowolski, R., and Staszczuk, P. (1999). On the Adsorption of Chromium (VI) Ions on Dolomite and 'Dolomitic Sorbents'. *Adsorption Science and Technology 18*, 107-115. https://doi.org/10.1260/0263617001493323

Domenzain, J., Castro, J. and Galicia, L. (2016). Removal of RB5 dye using a Mexican natural zeolite: Characterization and evaluation. *International Journal 7*, 1169-1178.

Dutta Majumdar, J., and Manna, I. (2003). Laser processing of materials. *Sadhana 28*, 495-562. https://doi.org/10.1007/BF02706446

Fuentes, S., and Díaz, G. (1997). *Catalizadores ¿La Piedra Filosofal del Siglo XX?* 3° Edición, Colec. La Ciencia para todos. Fondo de Cultura Económica, 66.

Gelover, S., and Montes, A. (2014). *Eliminación de Contaminantes Orgánicos Emergentes Mediante Fotocatálisis Heterogénea con TiO_2, Empleando Luz Solar*. Coordinación de tratamiento y calidad del agua, Subcoordinación de potabilización, SEMARNAT. 31.

Ghaedi, M., Hajjati, S., Mahmudi, Z., Tyagi, I., Agarwal, S., Maity, A., & Gupta, V. K. (2015). Modeling of competitive ultrasonic assisted removal of the dyes - Methylene blue and Safranin-O using Fe_3O_4 nanoparticles. *Chemical Engineering Journal 268*, 28-37. https://doi.org/10.1016/j.cej.2014.12.090

Giraldo, L. F. G., Franco, E. A. M., and Arango, J. J. S. (2004). La fotocatálisis como alternativa para el tratamiento de aguas residuales. *Revista Lasallista de Investigación 1*, 83-92.

Golka, K., Kopps, S., and Myslak, Z. W. (2004). Carcinogenicity of azo colorants: Influence of solubility and bioavailability. *Toxicology Letters 151*, 203-210. https://doi.org/10.1016/j.toxlet.2003.11.016

Gupta, V. K., Atar, N., Yola, M. L., Üstündağ, Z., and Uzun, L. (2014). A novel magnetic FeAu core-shell nanoparticles anchored graphene oxide recyclable nanocatalyst for the reduction of nitrophenol compounds. *Water Research 48*, 210-217. https://doi.org/10.1016/j.watres.2013.09.027

Gupta, V. K., Jain, R., Nayak, A., Agarwal, S., and Shrivastava, M. (2011). Removal of the hazardous dye-Tartrazine by photodegradation on titanium dioxide surface. *Materials Science and Engineering C 31*, 1062-1067. https://doi.org/10.1016/j.msec.2011.03.006

Gupta, V. K., Kumar, R., Nayak, A., Saleh, T. A., and Barakat, M. A. (2013). Adsorptive removal of dyes from aqueous solution onto carbon nanotubes: A review. *Advances in Colloid and Interface Science 193-194*, 24-34. https://doi.org/10.1016/j.cis.2013.03.003

Gupta, V. K., Nayak, A., and Agarwal, S. (2015). Bioadsorbents for remediation of heavy metals: Current status and their future prospects. *Environmental Engineering Research 20*, 1-18. https://doi.org/10.4491/eer.2015.018

Gupta, V. K., Nayak, A., Agarwal, S., and Tyagi, I. (2014). Potential of activated carbon from waste rubber tire for the adsorption of phenolics: Effect of pre-treatment conditions. *Journal of Colloid and Interface Science 417*, 420-430. https://doi.org/10.1016/j.jcis.2013.11.067

Kaneva, N., Bojinova, A., and Papazova, K. (2016). Photocatalytic degradation of Reactive Black 5 and Malachite Green with ZnO and lanthanum doped nanoparticles. *Journal of Physics: Conference Series 682*. https://doi.org/10.1088/1742-6596/682/1/012022

Karthikeyan, S., Gupta, V. K., Boopathy, R., Titus, A., and Sekaran, G. (2012). A new approach for the degradation of high concentration of aromatic amine by heterocatalytic Fenton oxidation: Kinetic and spectroscopic studies. *Journal of Molecular Liquids 173*, 153-163. https://doi.org/10.1016/j.molliq.2012.06.022

Khani, H., Rofouei, M. K., Arab, P., Gupta, V. K., and Vafaei, Z. (2010). Multi-walled carbon nanotubes-ionic liquid-carbon paste electrode as a super selectivity sensor: Application to potentiometric monitoring of mercury ion(II). *Journal of Hazardous Materials 183*, 402-409. https://doi.org/10.1016/j.jhazmat.2010.07.039

Lucas, M. S., and Peres, J. A. (2006). Decolorization of the azo dye Reactive Black 5 by Fenton and photo-Fenton oxidation. *Dyes and Pigments 71*, 236-244. https://doi.org/10.1016/j.dyepig.2005.07.007

Luna, R. A., Zermeño, B. B., Moctezuma, E., Contreras, R. E., Leyva, E., and López, M. A. (2013). Fotodegradación de omeprazol en solucín acuosa utilizando TiO_2 como catalizador. *Revista Mexicana de Ingeniera Qumica 12*, 85-95.

Luxon, J. T., and Parker, D. E. (1984). *Industrial Laser and Their Application*. N. J. 07632 Prentice-Hall, INC, Englewood Cliffs, Ed.

Mahmoodi, N. M., Arami, M., and Limaee, N. Y. (2006). Photocatalytic degradation of triazinic ring-containing azo dye (Reactive Red 198) by using immobilized TiO_2 photoreactor: Bench scale study. *Journal of Hazardous Materials 133*, 113-118. https://doi.org/10.1016/j.jhazmat.2005.09.057

Martínez, J., Membillo I. and Martínez, A. (2018). Decolorization of reactive black 5 immobilized. *Revista Mexicana de Ingeniería Química 10*, 17-28.

Mittal, A., Mittal, J., Malviya, A., and Gupta, V. K. (2010). Removal and recovery of Chrysoidine Y from aqueous solutions by waste materials. *Journal of Colloid and Interface Science 344*, 497-507. https://doi.org/10.1016/j.jcis.2010.01.007

Mohammadi, N., Khani, H., Gupta, V. K., Amereh, E., and Agarwal, S. (2011). Adsorption process of methyl orange dye onto mesoporous carbon material-kinetic and thermodynamic studies. *Journal of Colloid and Interface Science 362*, 457-462. https://doi.org/10.1016/j.jcis.2011.06.067

Moreno-Virgen, M. R., Soto-Bernal, J. J., Ortiz-Lozano, J. A., Bonilla-Petriciolet, A., Vega-Durán, J. T., González-Mota, R., and Pineda-Piñon, J. (2011). Influencia de la radiación láser de CO; en las propiedades mecánicas de pastas de cemento portland. *Materiales de Construcción 61*, 77-91. https://doi.org/10.3989/mc.2010.54709

Muruganandham, M., and Swaminathan, M. (2004). Photochemical oxidation of reactive azo dye with UV-H_2O_2 process. *Dyes and Pigments 62*, 269-275. https://doi.org/10.1016/j.dyepig.2003.12.006

Nagarathnam, K. (2001). Technology assessment of laser-assisted materials processing in space. *AIP Conference Proceedings 552*, 153-160. https://doi.org/10.1063/1.1357920

Nematollahzadeh, A., Shojaei, A., and Karimi, M. (2015). Chemically modified organic/inorganic nanoporous composite particles for the adsorption of reactive black 5 from aqueous solution. *Reactive and Functional Polymers 86*, 269-281. https://doi.org/10.1016/j.reactfunctpolym.2014.11.001

Pawlowski, L. (1999). Thick laser coatings: A review. *Journal of Thermal Spray Technology 8*, 279-295. https://doi.org/10.1361/105996399770350502

Rajendran, S., Khan, M. M., Gracia, F., Qin, J., Gupta, V. K., and Arumainathan, S. (2016). Ce^{3+}-ion-induced visible-light photocatalytic degradation and electrochemical activity of ZnO/CeO_2 nanocomposite. *Scientific Reports 6*, 31641. https://doi.org/10.1038/srep31641

Robati, D., Mirza, B., Rajabi, M., Moradi, O., Tyagi, I., Agarwal, S., and Gupta, V. K. (2016). Removal of hazardous dyes-BR 12 and methyl orange using graphene oxide as an adsorbent from aqueous phase. *Chemical Engineering Journal 284*, 687-697. https://doi.org/10.1016/j.cej.2015.08.131

Salas, G. (2010). Tratamiento por oxidación avanzada (Reacción Fenton) de aguas residuales de la industria textil. *Revista Peruana de Química e Ingeniería Química 13*, 30-38.

Saleh, T. A., and Gupta, V. K. (2011). Functionalization of tungsten oxide into MWCNT and its application for sunlight-induced degradation of rhodamine B. *Journal of Colloid and Interface Science 362*, 337-344. https://doi.org/10.1016/j.jcis.2011.06.081

Saleh, T. A., and Gupta, V. K. (2012a). Photo-catalyzed degradation of hazardous dye methyl orange by use of a composite catalyst consisting of multi-walled carbon nanotubes and titanium dioxide. *Journal of Colloid and Interface Science 371*, 101-106. https://doi.org/10.1016/j.jcis.2011.12.038

Saleh, T. A., and Gupta, V. K. (2012b). Synthesis and characterization of alumina nano-particles polyamide membrane with enhanced flux rejection performance. *Separation and Purification Technology 89*, 245-251. https://doi.org/10.1016/j.seppur.2012.01.039

Saleh, T. A., and Gupta, V. K. (2014). Processing methods, characteristics and adsorption behavior of tire derived carbons: A review. *Advances in Colloid and Interface Science 211*, 93-101. https://doi.org/10.1016/j.cis.2014.06.006

Saravanan, R., Gupta, V. K., Prakash, T., Narayanan, V., and Stephen, A. (2013). Synthesis, characterization and photocatalytic activity of novel Hg doped ZnO nanorods prepared by thermal decomposition method.

Journal of Molecular Liquids 178, 88-93. https://doi.org/10.1016/j.molliq.2012.11.012

Saravanan, R., Joicy, S., Gupta, V. K., Narayanan, V., and Stephen, A. (2013). Visible light induced degradation of methylene blue using CeO_2/V_2O_5 and CeO_2/CuO catalysts. *Materials Science and Engineering C 33*, 4725-4731. https://doi.org/10.1016/j.msec.2013.07.034

Saravanan, R., Karthikeyan, N., Gupta, V. K., Thirumal, E., Thangadurai, P., Narayanan, V., and Stephen, A. (2013). ZnO/Ag nanocomposite: An efficient catalyst for degradation studies of textile effluents under visible light. *Materials Science and Engineering C 33*, 2235-2244. https://doi.org/10.1016/j.msec.2013.01.046

Saravanan, R., Karthikeyan, S., Gupta, V. K., Sekaran, G., Narayanan, V., and Stephen, A. (2013). Enhanced photocatalytic activity of ZnO/CuO nanocomposite for the degradation of textile dye on visible light illumination. *Materials Science and Engineering C 33*, 91-98. https://doi.org/10.1016/j.msec.2012.08.011

Saravanan, R., Mansoob Khan, M., Gupta, V. K., Mosquera, E., Gracia, F., Narayanan, V., and Stephen, A. (2015). ZnO/Ag/CdO nanocomposite for visible light-induced photocatalytic degradation of industrial textile effluents. *Journal of Colloid and Interface Science 452*, 126-133. https://doi.org/10.1016/j.jcis.2015.04.035

Saravanan, R., Mansoob Khan, M., Gupta, V. K., Mosquera, E., Gracia, F., Narayanan, V., and Stephen, A. (2015). ZnO/Ag/CdO nanocomposite for visible light-induced industrial textile effluents degradation, uric acid and ascorbic acid sensing and antimicrobial activities. *RSC 5*, 34645-34651. https://pubs.rsc.org/en/content/articlelanding/2015/ra/c4ra15637d#!divAbstract

Saravanan, R., Thirumal, E., Gupta, V. K., Narayanan, V., and Stephen, A. (2013). The photocatalytic activity of ZnO prepared by simple thermal decomposition method at various temperatures. *Journal of Molecular Liquids 177*, 394-401. https://doi.org/10.1016/j.molliq.2012.10.018

Sasaki, K., Qiu, X., Hosomomi, Y., Moriyama, S., and Hirajima, T. (2013). Effect of natural dolomite calcination temperature on sorption of borate onto calcined products. *Microporous and Mesoporous Materials 171*, 1-8. https://doi.org/10.1016/j.micromeso.2012.12.029

Settanni, G., Zhou, J., Suo, T., Schöttler, S., Landfester, K., Schmid, F., & Mailänder, V. (2017). Protein corona composition of poly(ethylene glycol)- and poly(phosphoester)-coated nanoparticles correlates strongly with the amino acid composition of the protein surface. *Nanoscale 9*, 2138-2144. https://doi.org/10.1039/C6NR07022A

Sheet-Alabdraba W.M. and Ali Albayati M. B. (2014). Biodegradation of azo dyes a review biodegradation of azo dyes a review. *International Journal of Environmental Engineering and Natural Resources 1*, 179-189.

Stambolova, I., Shipochka, M., Blaskov, V., Loukanov, A., and Vassilev, S. (2012). Sprayed nanostructured TiO_2 films for efficient photocatalytic degradation of textile azo dye. *Journal of Photochemistry and Photobiology B: Biology 117*, 19-26. https://doi.org/10.1016/j.jphotobiol.2012.08.006

Vaidya A.A. and Datye K.V. (1982). Environmental pollution during chemical processing of synthetic fibers. *Colourage 14*, 3-10.

Vergara, J., Pérez, J. P., Suárez, R., and Hernández, I. (2012). Degradation of reactive red 120 azo dye in aqueous solutions using homogeneous/heterogeneous iron systems. *Revista Mexicana de Ingeniería Química 11*, 121-131.

Zollinger H. (1987). *Color Chemistry – Syntheses, Properties and Applications of Organic Dyes Pigments*. VCH, New York, NY.